

Infrared features of unquenched finite temperature lattice Landau gauge QCD

Sadataka Furui*

School of Science and Engineering, Teikyo University, 320-8551 Japan.

Hideo Nakajima†

Department of Information Science, Utsunomiya University, 321-8585 Japan.

(Dated: December 2, 2024)

The color diagonal and color antisymmetric ghost propagators slightly above T_c of $N_f = 2$ MILC $24^3 \times 12$ lattices are measured and compared with zero temperature unquenched $N_f = 2 + 1$ MILC $20^3 \times 64$ and MILC $28^3 \times 96$ lattices and zero temperature quenched 56^4 $\beta = 6.4$ and 6.45 lattices. The expectation value of the color antisymmetric ghost propagator $\phi^c(q)$ is zero but its Binder cumulant, which is consistent with that of $N_c^2 - 1$ dimensional Gaussian distribution below T_c , decreases above T_c . Although the color diagonal ghost propagator is temperature independent, the l^1 norm of the color antisymmetric ghost propagator is temperature dependent. The expectation value of the ghost condensate observed at zero temperature unquenched configuration is consistent with 0 in $T > T_c$.

We also measure transverse, magnetic and electric gluon propagator and extract gluon screening masses. The running coupling measured from the product of the gluon dressing function and the ghost dressing function are almost temperature independent but the effect of A^2 condensate observed at zero temperature is consistent with 0 in $T > T_c$.

The transverse gluon dressing function at low temperature has a peak in the infrared but it becomes flatter at high temperature. Its absolute value in the high momentum is larger for high temperature and similar to the magnetic gluon dressing function. The electric gluon propagator at high momentum is temperature independent. These data imply that the magnetic gluon propagator and the color antisymmetric ghost propagator are affected by the presence of dynamical quarks and there are strong non-perturbative effects through the temperature dependent color anti-symmetric ghost propagator.

PACS numbers: 12.38.Gc, 12.38.Aw, 11.10.Gh, 11.15.Ha, 11.15.Tk, 11.30.Rd

I. INTRODUCTION

As a condition of the color confinement in the infrared region, Kugo-Ojima criterion[1] and the Gribov-Zwanziger scenario[2, 3] are well-known. In these theories, infrared divergence of the ghost propagator is the essential ingredient of the emergence of the string-like inter-quark potential. In finite temperature SU(2) lattice Coulomb gauge simulation, linearly rising color-Coulomb potential was observed to remain above the deconfinement temperature T_c [4]. The color-Coulomb potential is defined by the ghost propagator and the color diagonal ghost propagator is found to be essentially temperature independent. The temperature dependence of the color antisymmetric ghost propagator was not explored. Coulomb gauge is a non-covariant gauge and the momentum in the time direction is not affected by the gauge fixing. In finite temperature, the momentum in the time direction is interpreted as the Matsubara frequency with appropriate boundary conditions.

The Landau gauge is a covariant gauge, and in the analysis of the quenched and unquenched lattice Lan-

dau gauge simulation[5, 6], we observed that the Kugo-Ojima parameters of the zero temperature unquenched configuration of the SU(3) MILC collaboration of $20^3 \times 64$ $\beta_{imp} = 6.76, 6.83$ (MILC_c), and $28^3 \times 96$ $\beta_{imp} = 7.09, 7.11$ (MILC_f) are consistent with 1 while the quenched configuration of 56^4 lattice remained about 0.8. The Binder cumulant of the color anti-symmetric ghost propagator of the zero temperature quenched SU(2) and unquenched SU(3) configurations of the MILC collaboration were consistent with those the $N_c^2 - 1$ dimensional Gaussian distribution, where N_c is the number of colors. The dynamical quark has the effect of quenching randomness of the system.

In this paper, we extend the analysis of the color anti-symmetric ghost propagator to the quenched SU(3) 56^4 lattices of $\beta = 6.4$ [6] and 6.45 [7] and the finite temperature unquenched SU(3) $24^3 \times 12$ configurations of the MILC collaboration[8]. The ghost propagator contributes in the off-shell quark gluon vertex via Ward-Slavnov-Taylor identity[9], and so we expect the screening masses of the gluons produced by the quark loops and ghost loops would be affected by the ghost propagator. We study the magnetic and the electric screening mass of the gluon of the MILC finite temperature $N_f = 2$ configurations of $\beta = 5.65, 5.725, 5.85$.

In the analysis of [10], the three configurations correspond to the temperature $T = 143, 172.5$ and 185 MeV _{ρ} , respectively where subscript ρ means that the scale is

*Electronic address: furui@umb.teikyo-u.ac.jp;
URL: http://albert.umb.teikyo-u.ac.jp/furui_lab/furuiPBS.htm

†Electronic address: nakajima@is.utsunomiya-u.ac.jp

fixed from the mass of the ρ meson $m_\rho = 770\text{MeV}$, and the temperature T_c that the cross over to the deconfinement occurs was assigned to be about 140MeV from the data of chiral susceptibility. Since the standard Wilson plaquette action was used in the production of the gauge configuration, the flavor symmetry was broken and the ratio of the ρ mass to pion mass is larger than the physical value[11]. Recent simulation with Asqtad action[12] suggests that $T_c \sim 170\text{MeV}$, consistent with the value of that of $N_f = 2$ improved Kogut-Susskind (KS) fermion $T_c \sim 173 \pm 8\text{MeV}$ [13]. A systematic comparison of the ρ meson mass for improved staggered actions in quenched approximation is given in [16]. Recently, [15] claims that the transition temperature depends on which physical quantity one measures, and that the T_c defined by the chiral susceptibility is $151(3)\text{MeV}$ and consistent within errors with [10]. They showed that the T_c defined by the strange quark chiral susceptibility and the Polyakov loop are about 175MeV and consistent with [13].

Since the continuum limit of the mass of the vector meson would not depend on the temperature near T_c [14], it would be natural to assign the bare lattice ρ mass by about 20% heavier and shift the temperature by the same amount. We leave a more accurate assignment of the temperature scale of the MILC_{ft} to a future study and assign the $\beta = 5.65, 5.725$ and 5.85 data by $T/T_c = 1.02, 1.23$ and 1.32 , respectively. We compare quenched and unquenched ghost propagator of zero temperature and finite temperature and investigate the role of quarks on the gluon field and its dependence on the temperature.

The organization of the paper is as follows. In the Sect.2, we show the results of the color diagonal ghost propagator of the quenched 56^4 and unquenched finite temperature MILC configurations. The corresponding color antisymmetric ghost propagators are shown in the Sect.3. The Kugo-Ojima parameters, the transverse, magnetic and electric gluon propagator and the QCD running coupling of the finite temperature unquenched configurations are shown in the Sects.4, 5 and 6, respectively. Conclusions and a discussion are given in the Sect.7

II. THE COLOR DIAGONAL GHOST PROPAGATOR

The ghost propagator is defined by the Fourier transform (FT) of the expectation value of the inverse Faddeev-Popov (FP) operator $\mathcal{M} = -\partial_\mu D_\mu$, where D_μ is the covariant derivative, as

$$\begin{aligned} FT[D_G^{ab}(x, y)] &= FT\langle \text{tr}(\Lambda^{a\dagger} \{(\mathcal{M}[U])^{-1}\}_{xy} \Lambda^b) \rangle, \\ &= \delta^{ab} D_G(q^2). \end{aligned} \quad (1)$$

where U is the link variable obtained by the Landau gauge fixing. In all the simulation in this work we adopt the $\log U$ definition of the gauge field, and the $\text{SU}(3)$ color matrix Λ is normalized as $\text{tr} \Lambda^a \Lambda^b = \delta^{ab}$. Number

of samples is about 10 each in the 56^4 lattices and about 100 each in the $24^3 \times 12$ lattices.

In the usual Monte Carlo simulation, it is necessary to make an average over many samples, but the color diagonal ghost propagator and the color anti-symmetric ghost propagator of unquenched configurations are almost independent of samples. Since we adopt the cylinder cut, i.e. select the momentum along the diagonal direction in momentum space, and take into account translation invariance and rotational symmetry of the lattice, the error bar of the ghost propagator of one sample is already not so large, and an order of 10 samples is enough to get the expectation values, although one should be cautious to the appearance of exceptional samples[6].

The color diagonal ghost propagator is defined as

$$\begin{aligned} D_G(q) &= \frac{1}{N_c^2 - 1} \frac{1}{V} \\ &\times \text{tr} \langle \delta^{ab} (\langle \Lambda^a \cos \mathbf{q} \cdot \mathbf{x} | f_c^b(\mathbf{x}) \rangle + \langle \Lambda^a \sin \mathbf{q} \cdot \mathbf{x} | f_s^b(\mathbf{x}) \rangle) \rangle \\ &= G(q^2)/q^2 \end{aligned}$$

Here $f_c^b(\mathbf{x})$ and $f_s^b(\mathbf{x})$ are the solution of $\mathcal{M} f^b(\mathbf{x}) = \rho^b(\mathbf{x})$ with $\rho^b(\mathbf{x}) = \frac{1}{\sqrt{V}} \Lambda^b \cos \mathbf{q} \cdot \mathbf{x}$ and $\frac{1}{\sqrt{V}} \Lambda^b \sin \mathbf{q} \cdot \mathbf{x}$, respectively.

A. Quenched $\text{SU}(3)$ 56^4 lattice

The color diagonal ghost propagators of 56^4 quenched $\text{SU}(3)$ are shown in [6], but we show the data for a comparison with the color anti-symmetric ghost propagator in the next subsection. The FIG. 1 is the ghost dressing function, of the 56^4 $\beta = 6.45$ configurations produced by the Monte Carlo simulation and subsequently Landau gauge fixed.

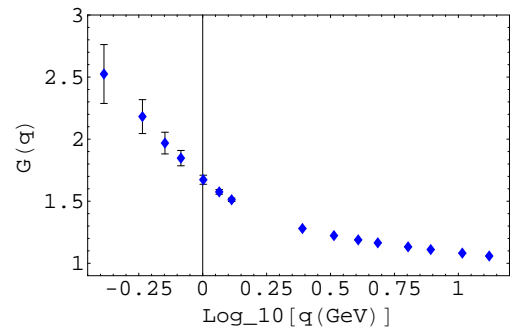


FIG. 1: The ghost dressing function of quenched 56^4 configurations of $\beta = 6.45$ as the function of $\log_{10}[q(\text{GeV})]$.

The scale of the $\beta = 6.4$ and 6.45 configurations are fixed as in TABLE I, using the formula in [17]. The ghost propagator is infrared divergent, but its singularity is weaker than q^{-4} .

TABLE I: β_{imp}/β , the inverse lattice spacing $1/a$, lattice size and lattice length(fm) of configurations investigated in this paper. Subscripts c and f of MILC correspond to coarse lattice($a=0.12\text{fm}$) and fine lattice($a=0.09\text{fm}$). $\beta_{imp} = 5/3 \times \beta$.

	β_{imp}/β	am_{ud}/am_s	N_f	$1/a(\text{GeV})$	L_s	L_t	$aL_s(\text{fm})$
quench	6.4		0	3.66	56	56	2.96
	6.45		0	3.87	56	56	2.94
MILC _c	6.83	0.040/0.050	2+1	1.64	20	64	2.41
	6.76	0.007/0.050	2+1	1.64	20	64	2.41
MILC _f	7.11	0.0124/0.031	2+1	2.19	28	96	2.52
	7.09	0.0062/0.031	2+1	2.19	28	96	2.52
MILC _{ft}	5.65	0.008	2	1.716	24	12	2.76
	5.725	0.008	2	1.914	24	12	2.47
	5.85	0.008	2	2.244	24	12	2.11

B. MILC finite temperature $24^3 \times 12$ lattice

The color diagonal ghost dressing function of MILC finite temperature configurations are shown in FIG. 2. We observe that the three data of different temperatures scale as shown in the figure when each lattice spacing a is chosen as in the ref.[10].

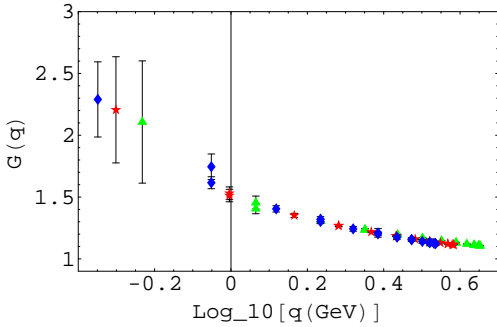


FIG. 2: The ghost dressing function of MILC_{ft} configurations of $T/T_c = 1.02$ (blue diamonds), $T/T_c = 1.23$ (red stars) and $T/T_c = 1.32$ (green triangles) as the function of $\log_{10}[q(\text{GeV})]$.

III. THE COLOR ANTISYMMETRIC GHOST PROPAGATOR

The color anti-symmetric ghost propagator is defined as

$$\phi^c(q) = \frac{1}{N} \frac{1}{V} \times \text{tr} \langle f^{abc} (\langle \Lambda^a \cos \mathbf{q} \cdot \mathbf{x} | f_s^b(\mathbf{x}) \rangle - \langle \Lambda^a \sin \mathbf{q} \cdot \mathbf{x} | f_c^b(\mathbf{x}) \rangle) \rangle$$

where the outer-most bracket means the ensemble average.

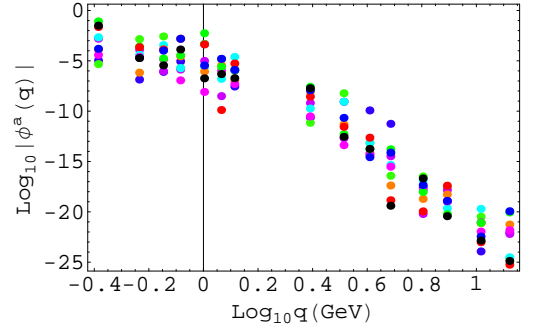


FIG. 3: $\log_{10} |\vec{\phi}(q)|$ as the function of $\log_{10} q(\text{GeV})$ of quenched $\beta = 6.45, 56^4$ lattice.

In a theory based on the Curci-Ferrari gauge and in its extension to the Landau gauge, a parameterization of the color anti-symmetric ghost propagator with use of the ghost condensate parameter v was proposed[18]. A simulation in the SU(2) lattice Landau gauge using a parameterization

$$\frac{1}{N_c^2 - 1} \sum_a |\phi^a(q)| = \frac{r/L^2 + v}{q^4 + v^2} \quad (2)$$

is performed in [19] and that of the zero temperature MILC_c and MILC_f are performed in [7, 20].

Another quantity that characterizes the system is the Binder cumulant of the color antisymmetric ghost propagator defined as

$$U(q) = 1 - \frac{\langle \vec{\phi}(q)^4 \rangle}{3 \langle \vec{\phi}(q)^2 \rangle^2}.$$

A simulation of SU(2) lattice Landau gauge obtained $U \sim 0.44$, almost independent of the momentum. This value is compatible with that of the three dimensional Gaussian distribution[20] and the analysis of SU(3) MILC_c and MILC_f showed that U is compatible with that of eight dimensional Gaussian distribution. We extend these analyses to large quenched lattices and the finite temperature configurations.

A. Quenched SU(3) 56^4 lattice

The absolute value of the color antisymmetric ghost propagator of quenched@ 56^4 lattice in the infrared region is about 3 orders of magnitude smaller than that of the color diagonal ghost propagator and the values are sample dependent. Results of $\beta = 6.45, 56^4$ 10 samples are shown in Fig.3.

Due to this sample dependence, quite different from the case of unquenched $20^3 \times 64$ lattices[20] and $28^3 \times 96$ [7], the Binder cumulant of the color antisymmetric ghost propagator of quenched configurations is noisy due

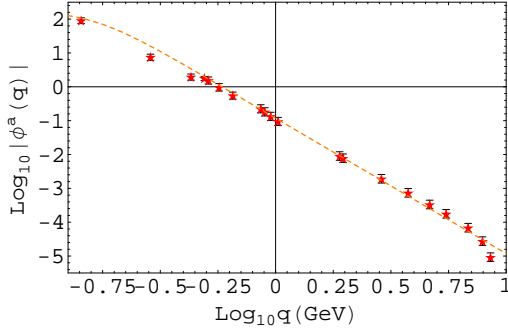


FIG. 4: $\log_{10} |\vec{\phi}(q)|$ as the function of $\log_{10} q(\text{GeV})$ of MILC_f and the fit using $r = 134$ and $v = 0.026\text{GeV}^2$.

to large $\langle \vec{\phi}(q)^4 \rangle$ as compared to $\langle \vec{\phi}(q)^2 \rangle^2$. The randomness of the color anti-symmetric ghost propagator of quenched configurations is large and the Binder cumulant becomes unstable.

B. MILC zero temperature $28^3 \times 96$ lattice

The color antisymmetric ghost propagator of MILC_f is shown in FIG. 4. Details of the fitting procedure are presented in [7]. We first fix the parameter r by the fit of $\frac{|\phi^a(q)|}{\cos(\pi\bar{q}/L)}$, where \bar{q} takes integer values $0, 1, \dots, L$, using the parameterization

$$\frac{1}{N_c^2 - 1} \sum_a \frac{L^2}{\cos(\pi\bar{q}/L)} |\phi^a(q)| = \frac{r}{q^z}, \quad (3)$$

and then fix v by the fit of $|\phi^a(q)|$ by eq.(2).

The expectation value of v is small but the condition that the fitted curve passes the lowest momentum point of Fig.4 within the error bar gives $v = 0.026(6)\text{GeV}^2$. It suggests that the presence of BRST partner of A^2 condensate at zero temperature.

The Binder cumulant of the zero temperature MILC_c lattice is reported in [20] and that of MILC_f is reported in [7]. We observed that the mass function of $m_0 = 27.2\text{MeV}$ quark propagator of $\beta_{imp} = 7.09$ with bare mass combination $m_0 = 27.2\text{MeV}/68\text{MeV}$ shows an anomalous behavior in $q < 1\text{GeV}$ region, and that in the same region Binder cumulant $U(q)$ shows an anomalous behavior, although the mass function of $m_0 = 68\text{MeV}$ does not show the anomaly. The non-QCD like behavior of staggered quarks calculated with large lattice spacing a and small bare mass m_0 is reported in [21]. Since no anomaly was observed in $\beta = 7.09$ $m_0 = 13.6\text{MeV}/68\text{MeV}$ [7, 22], effects of the relative size of the s -quark mass v , ud -quark mass and the number of N_f are suggested.

Thus we extend the analysis to MILC configuration of $N_f = 3$, $\beta_{imp} = 7.18$, $28^3 \times 96$ lattice with the bare quark mass $m_0 = 0.031$ and that of $N_f = 2$, $\beta_{imp} = 7.20$,

$20^3 \times 64$ lattice with the bare quark mass $m_0 = 0.02$ [31]. Preliminary results of the Binder cumulants of $N_f = 3$ and $N_f = 2$ are $0.66(1)$, i.e. $\langle \vec{\phi}(q)^4 \rangle$ is close to $\langle \vec{\phi}(q)^2 \rangle^2$. When the bare masses of the quarks are the same, the system possesses the self averaging property[32], and when they are different as in $N_f = 2 + 1$, the system lacks this property.

C. MILC finite temperature $24^3 \times 12$ lattice

The fluctuation of the color antisymmetric ghost propagator around the expectation value 0 was almost Gaussian in the case of zero temperature unquenched configurations[7, 20]. The logarithm of the absolute value of the color antisymmetric ghost propagator of finite temperature unquenched configurations as a function of the logarithm of the momentum is shown in the FIG. 5. In contrast to the color diagonal ghost propagator, the absolute value of the color antisymmetric ghost propagator depends on the temperature. The temperature dependence of the scale of ϕ defined by r of eq.(3) can be expressed as roughly $r \sim 5.49a^{-4.23}$, where a is the lattice spacing at each temperature in the unit of GeV.

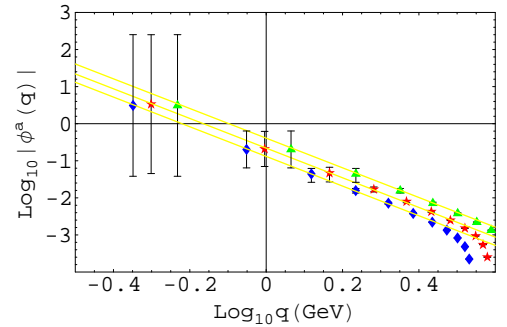


FIG. 5: $\log_{10} |\vec{\phi}(q)|$ as the function of $\log_{10} \bar{q}(\text{GeV})$ of MILC_{ft} of $T/T_c = 1.02$ (blue diamonds), $T/T_c = 1.23$ (red stars) and $T/T_c = 1.32$ (green triangles).

The fitting parameters of the color anti-symmetric ghost propagator are given in TABLE II. The condensate parameter v of finite temperature is difficult to assign since the lattice spacing is relatively large and difficult to detect the infrared bending behavior in the color anti-symmetric ghost propagator, but they are consistent with 0.

The Binder cumulant of ϕ is almost independent of the momentum except the lowest momentum point. We show a typical example of $T/T_c = 1.23$ in FIG. 6.

The temperature dependence of the average of $U(q)$ excluding the lowest momentum point is shown in FIG. 7. The average $U(T)$ decreases monotonically as a function of T from that of the Gaussian distribution (dashed line) at high temperature.

TABLE II: The fitted parameters r, z and v of the color antisymmetric ghost propagator $|\phi(q)|$ of MILC_c, MILC_f and MILC finite temperature. Two values of U of MILC_f correspond to the average below $q = 1\text{GeV}$ and the average above 1GeV , respectively.

β_{imp}/β	$m_0(\text{MeV})$	r	z	v	U
6.76	11.5/82.2	37.5	3.90	0.02(1)	0.53(5)
6.83	65.7/82.2	38.7	3.85	0.01(1)	0.57(4)
7.09	13.6/68.0	134	3.83	0.026(6)	0.57(4)/0.56(1)
7.11	27.2/68.0	112	3.81	0.028(8)	0.58(2)/0.52(1)
5.65	12.3	54.4	4.01	0.0	0.580(13)
5.725	12.8	88.3	3.95	0.0	0.571(4)
5.85	15.0	165.9	3.93	0.0	0.558(2)

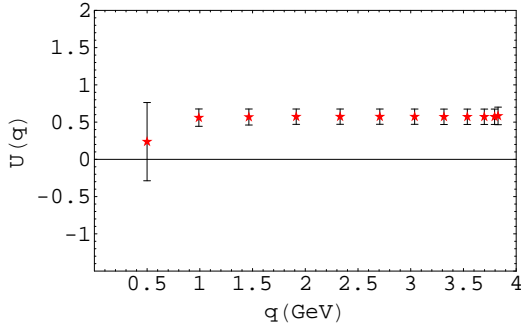


FIG. 6: The Binder cumulant of the color antisymmetric ghost propagator of MILC $N_f = 2$ configurations of $T/T_c = 1.23$ (red stars).

IV. THE KUGO-OJIMA COLOR CONFINEMENT PARAMETER

The Kugo-Ojima parameter is defined by the two point function of the covariant derivative of the ghost and the commutator of the antighost and gauge field

$$\begin{aligned} & \left(\delta_{\mu\nu} - \frac{q_\mu q_\nu}{q^2} \right) u^{ab}(q^2) \\ &= \frac{1}{V} \sum_{x,y} e^{-ip(x-y)} \left\langle \text{tr} \left(\Lambda^{a\dagger} D_\mu \frac{1}{-\partial D} [A_\nu, \Lambda^b] \right)_{xy} \right\rangle. \end{aligned} \quad (4)$$

Kugo and Ojima[1] showed that $u(0) = -1$ is a condition of the color confinement. Zwanziger[3] defined the horizon function h that is related to the Kugo-Ojima parameter $c = -u(0)$ as follows.

$$\begin{aligned} & \sum_{x,y} e^{-ip(x-y)} \left\langle \text{tr} \left(\Lambda^{a\dagger} D_\mu \frac{1}{-\partial D} (-D_\nu) \Lambda^b \right)_{xy} \right\rangle \\ &= G_{\mu\nu}(p) \delta^{ab} = \left(\frac{e}{d} \right) \frac{p_\mu p_\nu}{p^2} \delta^{ab} - \left(\delta_{\mu\nu} - \frac{p_\mu p_\nu}{p^2} \right) u^{ab}, \end{aligned}$$

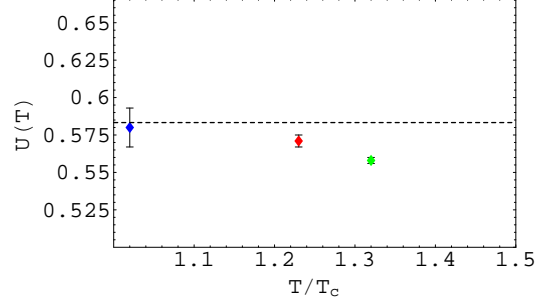


FIG. 7: Averages over momenta excluding the lowest momentum point of the Binder cumulants of MILC finite temperature configurations. $T/T_c = 1.02$ (blue diamonds), $T/T_c = 1.23$ (red stars) and $T/T_c = 1.32$ (green triangles).

where, with use of the covariant derivative $D_\mu(U)$

$$D_\mu(U_{x,\mu})\phi = S(U_{x,\mu})\partial_\mu\phi + [A_{x,\mu}, \bar{\phi}],$$

$$\partial_\mu\phi = \phi(x + \mu) - \phi(x), \quad \bar{\phi} = \frac{\phi(x + \mu) + \phi(x)}{2} \quad \text{and}$$

$$S(U_{x\mu}) = \frac{adj A_{x,\mu}/2}{\tanh(adj A_{x,\mu}/2)}.$$

Using the definition

$$e = \left\langle \sum_{x,\mu} \text{tr}(\Lambda^{a\dagger} S(U_{x,\mu}) \Lambda^a) \right\rangle / \{(N_c^2 - 1)V\},$$

the horizon condition reads $\lim_{p \rightarrow 0} G_{\mu\mu}(p) - e = 0$, and the

left hand side of the condition is $\left(\frac{e}{d}\right) + (d-1)c - e = (d-1)h$ where $h = c - \frac{e}{d}$ and dimension $d = 4$, and it follows that $h = 0 \rightarrow$ horizon condition, and thus the horizon condition coincides with Kugo-Ojima criterion provided the covariant derivative approaches the naive continuum limit, i.e., $e/d = 1$.

A. Quenched SU(3) 56^4 lattice

The Kugo-Ojima confinement parameter of quenched configuration saturates at about 80% of the expected value $c = 1$. There appear exceptional samples with an average consistent with $c = 1$ within errors. The polarization dependence of the Kugo-Ojima parameter of $\beta = 6.45$ samples is shown in FIG. 8.

B. MILC finite temperature $N_f = 2$, $24^3 \times 12$ lattice

Shown in TABLE III are the Kugo-Ojima parameters and the horizon function deviation of quenched 56^4 configurations, zero-temperature unquenched MILC_c and MILC_f configurations and unquenched finite temperature MILC_{ft} configurations.

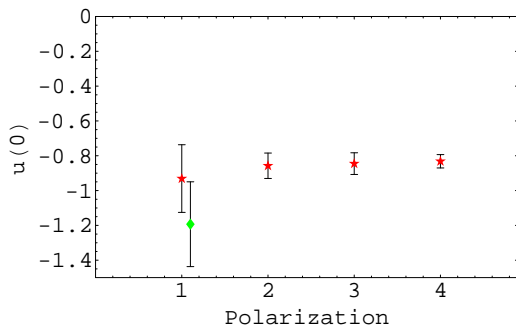


FIG. 8: Kugo-Ojima parameter $u(0)$ of quenched 56^4 configurations of $\beta = 6.45$ (red stars). The data of an exceptional sample is indicated by the green diamond. Polarizations 1,2,3,4 correspond to x, y, z and t .

The Kugo-Ojima parameters of unquenched zero-temperature configurations are consistent with the theory[7, 20, 23], and those of unquenched finite temperature configurations show temperature dependence.

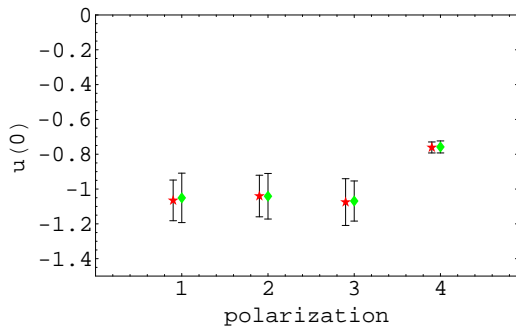


FIG. 9: Kugo-Ojima parameter $u(0)$ of MILC_f $N_f = 2 + 1$ KS fermion unquenched configurations of $\beta_{imp} = 7.11$ (green diamonds), $\beta_{imp} = 7.09$ (red stars).

The FIG. 9 show the dependence on the polarization of the Kugo-Ojima parameter. The polarization dependence of the parameter c is a result of an integration over the axes perpendicular to the polarization. It becomes large when there is a long axis perpendicular to the polarization. The FIG. 10 shows the temperature and the polarization dependence of the Kugo-Ojima parameter.

The quenched configurations and high temperature configurations show larger deviation from $u(0) = -1$, which would be due to higher randomness of these systems. The origin of the randomness in the latter would be the thermal fluctuation and that of the former would be lack of fermions that quench randomness of the system.

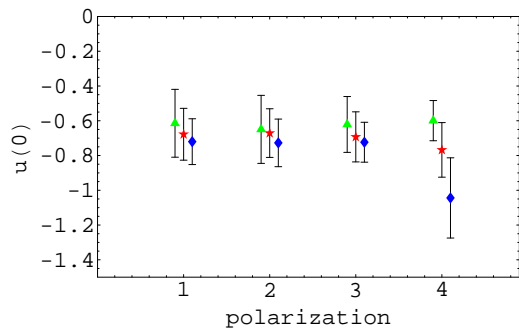


FIG. 10: Kugo-Ojima parameter $u(0)$ of MILC_{ft} configurations of $T/T_c = 1.02$ (blue diamonds), $T/T_c = 1.23$ (red stars) and $T/T_c = 1.32$ (green triangles).

V. THE FINITE TEMPERATURE GLUON PROPAGATOR

The fluctuation of the gluon propagators of lattice Landau gauge is larger than that of the ghost propagator. We measure the gluon propagators of the three temperature by using about 100 samples each and choosing the momenta along the three dimensional (3-d) coordinate axes and along the diagonal in the 3-d space. The dependence on the choice of the direction is not significant except a slight suppression of the $\vec{q} = (1, 1, 1, 0)$, as compared to that with the same magnitude but along the coordinate axes. We fix the normalization of the gluon propagator such that the running coupling defined by the product of the gluon dressing function and the ghost dressing function squared as defined in Sect. VI in the high momentum region agrees with the pQCD result and that the rescaling factor for the ghost dressing function and the gluon dressing function are the same. The renormalization factors defined by the highest momentum point along the coordinate axes of the three temperatures are 0.48(1).

In Fig. 11 the transverse gluon dressing functions of the three temperatures taken at momenta along the diagonal direction in the 3-d momentum space after the rescaling are shown. The asymptotic value of the lowest temperature is about 2, since we normalized $\text{Tr} \Lambda^a \Lambda^b = \delta^{ab}$. Larger values of the transverse gluon dressing function for higher temperature does not agree with a recent result of quenched SU(2) finite temperature simulation[35], but the qualitative momentum dependence i.e. infrared enhancement in the low temperature gluon dressing function agree with each other.

The temperature dependence of unquenched transverse gluon propagator and that of the magnetic gluon propagator $G_m(z)$, and the temperature dependence of the quenched SU(2) transverse gluon propagator[35] is similar to that of unquenched SU(3) electric gluon propagator $G_e(z)$, which are shown in Figs. 14 and 13, respectively.

The transverse gluon propagator at the zero momentum is finite as shown in Fig. 12. The value of $D_A(0)$ of

	β_{imp}/β	c_x	c_t	c	e/d	h
quenched	6.4			0.827(27)	0.954(1)	-0.12
	6.45			0.814(89)	0.954(1)	-0.14
MILC _c	6.76	1.04(11)	0.74(3)	0.97(16)	0.9325(1)	0.03(16)
	6.83	0.99(14)	0.75(3)	0.93(16)	0.9339(1)	-0.00(16)
MILC _f	7.09	1.06(13)	0.76(3)	0.99(17)	0.9409(1)	0.04(17)
	7.11	1.05(13)	0.76(3)	0.98(17)	0.9412(1)	0.04(17)
MILC _{ft}	5.65	0.72(13)	1.04(23)	0.80(21)	0.9400(7)	-0.14(21)
	5.725	0.68(15)	0.77(16)	0.70(15)	0.9430(2)	-0.24(15)
	5.85	0.63(19)	0.60(12)	0.62(17)	0.9465(2)	-0.33(17)

TABLE III: The Kugo-Ojima parameter of the quenched 56^4 lattice and that of the unquenched KS fermion (MILC_c, MILC_f, MILC_{ft}). c_x is the polarization along the spatial directions, c_t is that along the time direction, c is the average of c_x and c_t , e/d is the trace divided by the dimension and h is the horizon function deviation.

MILC_f, $\beta = 7.09$, $28^3 \times 96$ is about 15[23]. The $D_A(0)$ decreases monotonically as T decreases to 0. Whether it vanishes or remains finite is an important problem for fixing the nature of the infrared fixed point of the running coupling.

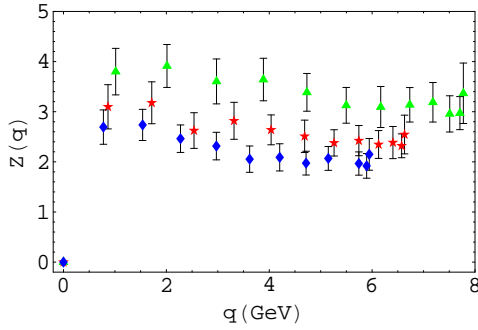


FIG. 11: The transverse gluon dressing function $Z(q)$ of MILC $N_f = 2$ KS fermion unquenched configuration of $T/T_c = 1.02$ (blue diamonds), $T/T_c = 1.23$ (red stars) and $T/T_c = 1.32$ (green triangles).

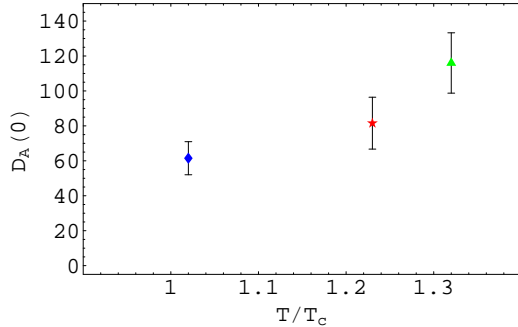


FIG. 12: The transverse gluon propagator of MILC $N_f = 2$ KS fermion unquenched configuration of $T/T_c = 1.02$ (blue diamonds), $T/T_c = 1.23$ (red stars) and $T/T_c = 1.32$ (green triangles) at $q = 0$.

We observe that the fluctuation of the gluon propagator at the zero momentum increases as the temperature increases.

The one-loop off-shell contribution to the quark-gluon vertex, is related to the quark-quark-ghost amplitude via Ward-Slavnov-Taylor identity[9]. The screening mass of the gluon would be affected by the ghost propagator. The correlation function of the gauge fields in the position space is defined as [24]

$$G_\mu(z) = \langle A_\mu(z) A_\mu(0) \rangle,$$

where $A_\mu(z) = \sum_{x_0, x_1, x_2} A_\mu(x_0, \vec{x})$.

The screening mass of the gluon is produced by the quark-, gluon- and ghost-loops. The electric screening mass m_e is defined by

$$G_e(z) = G_0(z) \sim \exp[-m_e z / N_t T]$$

The magnetic screening mass m_m is defined by

$$G_m(z) = (G_1(z) + G_2(z))/2 \sim \exp[-m_m z / N_t T]$$

We fit the propagator $G_e(z)$ and $G_m(z)$ by

$$G(z) = A \cosh[(m/N_t T)(z - N_x/2)].$$

The mass depends on the region of z used to fit the data and Karsch et al. proposed to fit data of z near $N_x/4$. [25] We fit the data from $z = 5$ to 9 . When we fit the data from $z = 0$ to $z = 6$, the masses become smaller by about 30-40%. Since deviations from the cosh functional form become larger in this region, we adopt the fit from $z = 5$ to 9 .

TABLE IV: The electric and the magnetic screening mass

β	T/T_c	m_e/T	m_m/T
5.65	1.02	3.42(27)	3.48(48)
5.725	1.23	3.22(40)	2.90(20)
5.85	1.32	3.14(33)	2.31(22)

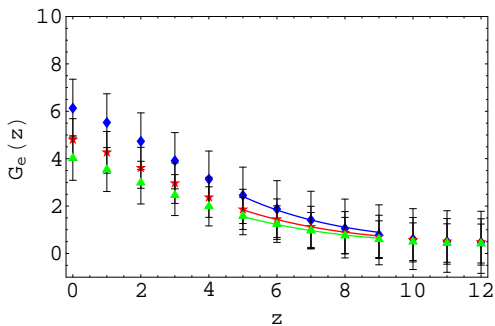


FIG. 13: Electric screening mass of MILC $N_f = 2$ KS fermion unquenched configuration of $T/T_c = 1.02$ (blue diamonds), $T/T_c = 1.23$ (red stars) and $T/T_c = 1.32$ (green triangles).

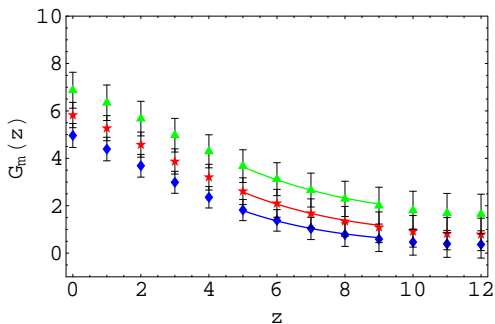


FIG. 14: Magnetic screening mass of MILC $N_f = 2$ KS fermion unquenched configurations of $T/T_c = 1.02$ (blue diamonds), $T/T_c = 1.23$ (red stars) and $T/T_c = 1.32$ (green triangles).

In high temperature, perturbative QCD (pQCD) suggests that

$$\frac{m_e}{T} \propto g(T), \frac{m_m}{T} \propto g^2(T)$$

where $g^2(T)/4\pi$ is the running coupling at temperature T and 0 momentum. Our electric screening mass and the magnetic screening mass are close to those of quenched SU(2) $m_e/T = 2.484(52)$ measured by [24]. The magnetic screening mass in the case of SU(2) using the data in the region of $T > 2T_c$ was $m_m/T = 0.466(25)g^2(T)$ in the two-loop pQCD calculation with $\Lambda_m = 0.262(18)T_c$. In the case of quenched SU(3), [26] obtained using the data in the region of $T > 1.5T_c$, $m_e/T = 1.69(4)g(T)$ and $m_m/T = 0.549(16)g^2(T)$. Since the electric and the magnetic gluon propagator of [26] are normalized to 1 at $z = 0$ and the critical temperature of the quenched configuration $T_c \sim 269 \pm 1 \text{ MeV}$ [13] is much higher than that of the unquenched configuration, we cannot compare quantitatively their data with ours, but their data of $T/T_c = 1.32$ are consistent with ours within errors. We do not observe suppression of m_e/T near T_c . Whether the discrepancy is due to the presence of dynamical quarks is left for the future study. Discrepancy of about

factor 6 in the m_m/T of SU(3) near T_c from the extrapolation of the pQCD results in $T > 1.5T_c$ region implies breakdown of the perturbation series near T_c .

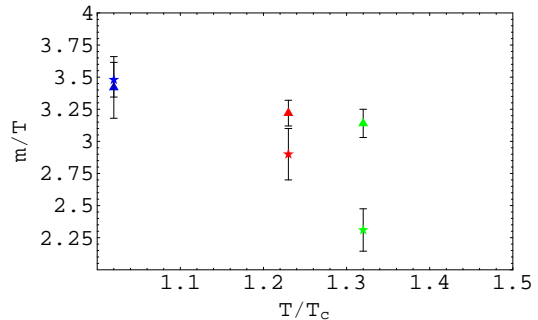


FIG. 15: The magnetic screening mass m_m/T (stars) and the electric screening mass m_e/T of MILC $N_f = 2$ KS fermion unquenched configurations (triangles).

VI. THE FINITE TEMPERATURE QCD RUNNING COUPLING

In [33] the calculation of the running coupling in the Dyson-Schwinger equation (DSE) at zero temperature [36] was extended to below T_c by using the ghost-gluon vertex $G_\nu(p, q) = -q_\nu$, where q and p are the incoming and outgoing ghost momentum, respectively. The running coupling for $q_0 = 2\pi nT$ is written as

$$\alpha(n, p_3^2, T) = \alpha(\mu^2) G^2(n, p_3^2, \mu^2, T) Z_3(n, p_3^2, \mu^2, T) \quad (5)$$

where $G(n, p_3^2, \mu^2, T)$ is the ghost dressing function and $Z_3(n, p_3^2, \mu^2, T)$ is the gluon dressing function. Applying this method to $T \sim T_c$, we measure the QCD running coupling in the \overline{MS} scheme as the product of the gluon dressing function and the ghost dressing function squared, as a function of the momentum \vec{q} along the spatial axes. We normalize the magnitude to the result of four-loop pQCD [23, 27, 28, 29] at the highest momentum point of $\beta = 5.725$. A DSE result of zero-temperature quenched configuration with the infrared exponent of the ghost propagator $\kappa = 0.5$ [30] and parameters used to fit the quenched simulation [6] is shown by the dashed line. The pQCD result of zero-temperature $N_f = 2$ system is shown by the dotted line.

Comparing with the result of $N_f = 2 + 1$ zero-temperature [23], the deviation from the pQCD is smaller. Although the presence of ghost condensate at zero temperature is not excluded, there is no sign of finite v and A^2 at finite temperature.

The running couplings of three temperatures near T_c as a function of the momentum \vec{q} lies roughly on a single curve and there is not strong temperature dependence. The relatively large T dependence of the m_m/T suggests that the non-perturbative effects on the magnetic screening mass is important.

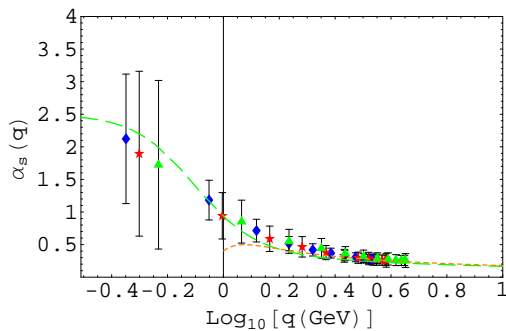


FIG. 16: The running coupling of the MILC finite temperature configurations of $\beta = 5.65$ (blue diamonds), 5.725 (red stars) and 5.85 (green triangles) as the function of $\log \bar{q}(\text{GeV})$. Dashed line is the DSE result used to fit the quenched zero temperature lattice data [6] with $\kappa = 0.5$ and the dotted line is the pQCD result with $N_f = 2$ of zero temperature.

VII. DISCUSSION AND CONCLUSION

We measured the color diagonal and the color antisymmetric ghost propagator of quenched, unquenched zero temperature and unquenched finite temperature configurations. The quark has the effect of quenching randomness of the ghost propagator and enhancing the transverse and magnetic gluon propagator above T_c . The Binder cumulant of the quenched SU(3) color antisymmetric ghost propagator is noisy, but that of the unquenched SU(3) color antisymmetric ghost propagator is almost constant and independent of the momentum except the lowest momentum point. The color diagonal ghost propagator of finite temperatures above T_c are almost temperature independent, but the scale of the color antisymmetric ghost propagator becomes larger as the temperature becomes higher.

We observed that the Binder cumulants of zero temperature unquenched $N_f = 2 + 1$ SU(N) configurations

are consistent with those of $N^2 - 1$ dimensional Gaussian distributions. The Binder cumulants of finite temperature unquenched $N_f = 2 + 1$ SU(3) configurations deviate from Gaussian distribution as the temperature rises, which may be interpreted as the quark effect of quenching randomness is reduced in high temperature. The anomaly of the KS fermion propagator and the anomaly of the momentum dependence of the Binder cumulant are correlated. It may indicate that the QCD-like region of $N_f = 2 + 1$ KS fermion system is more complicated than that of the $N_f = 2$ case given in [21]. The Binder cumulant of unquenched $N_f = 2$ and 3 which are consistent with 0.66 indicates that the ratio of the ud -quark mass and the s -quark mass is an important ingredient.

We observed strong non-perturbative effects in the magnetic screening mass of the gluon near T_c . Since near T_c , systematic perturbative QCD calculation is impossible, it is important to formulate the lattice theory. In the quenched finite temperature Landau gauge DSE approach [33, 34] the infrared exponent κ and the running coupling in the MOM scheme were found to be essentially temperature independent below T_c .

Acknowledgments

We thank F. Karsch for a discussion on the scale assignment of the lattice data and A. Nakamura and T. Saito for the information on the quenched simulation of their group. This work is supported by the High Energy Accelerator Research Organization (KEK) supercomputer project No. 05-128 using Hitachi-SR8000 and the large scale simulation program No.5(FY2006) using SR11000. Numerical calculation of the ghost propagator was carried out by NEC-SX5 at the CMC of Osaka University and by NEC-SX8 at the Yukawa Institute Computer Facility. H.N. is supported by the MEXT grant in aid of scientific research in priority area No.13135210.

-
- [1] T. Kugo and I. Ojima, Prog. Theor. Phys.(Kyoto) Suppl. **66**, 1 (1979).
 - [2] V.N. Gribov, Nucl. Phys. **B 139**(1978).
 - [3] D. Zwanziger, Nucl. Phys. **B 364**, 127 (1991), idem **B 412**, 657 (1994).
 - [4] J. Greensite, S. Olejník and D. Zwanziger, Phys. Rev. **D69**,074506(2004).
 - [5] S. Furui and H. Nakajima, Phys. Rev. **D69**,074505(2004); arXiv: hep-lat/0305010.
 - [6] S. Furui and H. Nakajima, Phys. Rev. **D70**,094504(2004); arXiv: hep-lat/0403021.
 - [7] S. Furui and H. Nakajima, Braz. J. Phys.**37**,Proceedings of IRQCD in Rio, June 5-9 2006, in press; arXiv:hep-lat/0609024.
 - [8] C. Bernard et al., Phys. Rev. **D58**,014503(1998).
 - [9] A.I. Davydychev, P. Osland and L. Saks, Phys. Rev. **D63**,014022(2000).
 - [10] C. Bernard et al., Phys. Rev. **D54**,4585(1996).
 - [11] T. Blum, L. Kärkkäinen, D. Toussaint and S. Gottlieb, Phys. Rev. **D51**,5153(1995).
 - [12] C. Bernard et al., hep-lat/0611031.
 - [13] F. Karsch and E. Laermann; arXiv: hep-lat/0305025.
 - [14] F. Karsch, in *Selected topics in non perturbative QCD*, "Enrico Fermi School". p.51-71 (1995); arXiv: hep-lat/9512029.
 - [15] Y. Aoki, Z. Fodor, S.D. Katz and K.K. Szabó, hep-lat/0609068 v2.
 - [16] M. Cheng, N.Christ, C. Jung, F. Karsch, R. Mawhinney, P. Petreczky and K. Petrov, hep-lat/0612030 v1.
 - [17] S. Necco and R. Sommer, Nucl. Phys. **B622**,328(2002); arXiv: hep-lat/0108008.
 - [18] D. Dudal et al., J. High Energy Phys. **06**, 003(2003).
 - [19] A.Cucchieri, T. Mendes and A. Mihara, Phys. Rev. **D72**,094505 (2005).

- [20] S. Furui and H. Nakajima, Phys. Rev. D **73**,094506(2006); arXiv:hep-lat/0602027.
- [21] A. Hasenfratz and R. Hoffmann, Phys. Rev. D **74**,014511(2006).
- [22] S. Furui and H. Nakajima, Phys. Rev. D **73**,074503(2006); arXiv:hep-lat/0511045.
- [23] S. Furui and H. Nakajima, Few Body Systems **40**,101 (2006) ; arXiv:hep-lat/0503029.
- [24] U.M. Heller, F. Karsch and J. Rank , Phys. Lett. B **355**,511(1995); arXiv: hep-lat/9505016.
- [25] U.M. Heller, F. Karsch and J. Rank , Phys. Rev. D **57**,1438(1998).
- [26] A. Nakamura, T. Saito and S. Sakai, Phys. Rev. D **69**,014506(2004).
- [27] Ph. Boucaud et al., JHEP **0201**,046 (2002) ; arXiv:hep-lat/0107278.
- [28] K.G. Chetyrkin and A. Rétyay ; arXiv:hep-ph/0007088; idem Nucl. Phys. B **583**,3(2000),arXiv:hep-ph/9910332.
- [29] K.G. Chetyrkin, Nucl. Phys. B **710**,499(2005); arXiv:hep-ph/0405193 v3(2005).
- [30] J.C. Bloch, Few Body Systems **33**,111 (2003).
- [31] C. Bernard et al., Phys. Rev. D **64** 054506, (2001); arXiv:hep-lat/0104002.
- [32] D.P. Landau and K. Binder, *A Guide to Monte Carlo Simulations in Statistical Physics*, Cambridge University Press. (2005).
- [33] B. Grüter, R. Alkofer, A. Maas and J. Wambach, Eur. Phys. J. C **42**, 109(2005); arXiv:hep-ph/0408282.
- [34] A. Maas, J. Wambach and R. Alkofer, Eur. Phys. J. C **42**, 93 (2005); arXiv:hep-ph/0504019.
- [35] A. Cucchieri, A. Maas and T. Mendes, hep-lat/0702022
- [36] L. von Smekal, A. Hauck and R. Alkofer, Ann. Phys.(N.Y.) **267**,1 (1998).